Quantum dots as fluorescence resonance energy transfer donors in cells

Nicole McGrath
Margarida Barroso
Albany Medical College
Center for Cardiovascular Sciences
Albany, New York 12208

Abstract. Quantum dots (QDs) promise to revolutionize the way fluorescence imaging is used in the cell biology field. The unique fluorescent spectral characteristics, high photostability, low photobleaching, and tight emission spectra of QDs position them above traditional dyes. We will address the ability of water-stabilized QDs to behave as effective fluorescence resonance energy transfer (FRET) donors in cells upon transferrin-receptor–(TFR) mediated endocytosis. Confocal microscopy detects whether donor QD transferrin conjugates transfer energy to acceptor organic fluorophore-transferrin conjugate molecules in endocytic compartments. QDs are shown to be effective FRET donors when internalized into cells via the transferring receptor-mediated endocytic pathway. Upon pairing with the appropriate acceptor dyes, QDs will reduce the laborious data processing that is required to compensate for bleed through contamination between organic dye donor and acceptor pair signals. The QD technology simplifies and expands the use of FRET in the analysis of complex cellular processes that may involve protein organization in intracellular membranes as well as protein-protein interactions. [DOI: 10.1117/1.2939417]

Keywords: quantum dots; fluorescence resonance energy transfer (FRET); transferrin; endocytic traffic.

Paper 07356SSR received Aug. 28, 2007; revised manuscript received Apr. 16, 2008; accepted for publication Apr. 17, 2008; published online Jun. 23, 2008.

1 Introduction

1.1 *Water-Stabilized Quantum Dots (QDs)*

QDs are semiconductor nanocrystals that have been used as powerful fluorescent tools for biological research.[1–4] The versatility of QD fluorescence stems from their small, tunable QD core sizes (1 to 10 nm). Both their emission and absorption spectra are related to the size of the QD core. QDs display very nearly Gaussian emission peaks, with no trace of the shoulders that plague most organic dye emission spectra. In contrast, QDs show broad absorption patterns. Narrow emission spectra together with broad absorption spectra make QDs very useful for fluorescence multiplexing. Furthermore, the photostability of QDs is greater than that of organic dyes at similar wavelengths. Here, we have used water-stabilized QDs, called EviTags (Evident Technologies; http://www.evidenttech.com/), that show a marked increase in performance capability over traditional organic dyes. EviTag QDs, generated using proprietary core-shell technology, have great stability and retention of high quantum yields and luminosities over long lifetimes. In addition to the core-related fluorescent properties, EviTag QDs have surface chemistries that add to their usefulness in biological research. Functionalized EviTag QDs can be easily conjugated to proteins, oligonucleotides, and other biomolecules using straightforward binding chemistries. Ligand-EviTag QD conjugates can be used to probe specific biological mechanisms in live and fixed cells and can be applied to immunoassays and a variety of other fluorescence-based detection assays, including fluorescence resonance energy transfer (FRET).

1.2 *FRET*

FRET is the radiationless transfer of energy from a donor fluorophore to an acceptor fluorophore in close proximity (1 to 10 nm) through dipole-dipole coupling.[5] For FRET to occur, the donor and acceptor fluorophores should have a sufficient spectral overlap between the donor emission and the acceptor absorption spectra, a favorable dipole-dipole orientation, a proximity of 1 to 10 nm, and a large enough quantum yield.[6–9] Upon energy transfer, the following events will occur: (1) donor fluorescence is quenched and acceptor fluorescence is increased (sensitized); (2) donor photobleaching rate is decreased; (3) donor excitation lifetime decreases; and (4) upon acceptor photobleaching, donor fluorescence is increased (unquenching). All these processes allow for the estimation of the energy transfer efficiency (E%). For a known donor-acceptor pair, E% provides a measure of spatial proximity since it decreases rapidly with increasing distance between the two fluorophores.[7,9,10]

One of the major shortcomings of using organic fluorophores, such as Alexa Fluor (AF) fluorophores, as donor and acceptor molecules, is that the spectral overlap between the

Address all correspondence to Margarida Barroso, Center for Cardiovascular Sciences, Albany Medical College, 47 New Scotland Ave., Albany, NY 12208-3479; Tel: 518 262 6435; FAX: 518 262 8101; E-mail: barrosm@mail.amc.edu

1083-3668/2008/13(3)/031210/9/$25.00 © 2008 SPIE

donor emission and the acceptor excitation spectra results in the contamination of the FRET signal due to the overlap between the donor and acceptor emission spectra (donor spectral bleedthrough, or DSBT) and to the donor excitation of the acceptor fluorophore (acceptor SBT, or ASBT). In the absence of a reliable correction method, small changes expressed in differential FRET signals may be misinterpreted, particularly where the FRET signal approaches the fluorescence level of the background contamination. There are a number of methods that attempt to minimize the SBT contamination, each with certain limitations, depending on the level of sensitivity desired.[11–17] The acceptor and donor photobleaching methods estimate E% while avoiding the need for SBT correction,[14,18] but they may cause unforeseen changes in the specimen as a result of significant laser power exposure.[19,20] Other approaches have been used to lessen the SBT contamination problem, such as spectral FRET imaging[21,22] and algorithm-based SBT correction of FRET intensity-based imaging.[23–27] Recently, we have developed a highly sensitive algorithm-based method precision FRET (PFRET) SBT correction algorithm to remove donor and acceptor SBT spillover from intensity-based FRET signals in a pixel-by-pixel manner, using single-labeled reference specimens.[23–31]

1.3 *Quantum Dots Used in Cellular Imaging and in FRET Applications*

Recent reports have shown that QDs can be used for *in vivo* cellular imaging, in particular, to follow the endocytosis of receptor-ligand complexes.[1–3,32–34] For example, QDs have been used to follow the binding of epidermal growth factor (EGF) to its receptor and elicit subsequent signal transduction events.[35] QDs have also been shown to be effective for the long-term labeling of endosomes.[36] These and other reports illustrate how QDs can be used without significant negative effects for long-term labeling of cells and organelles.[32,36]

QDs have been shown to act as strong FRET donors to dye acceptors in *in vitro* experiments, as reviewed in Ref. 37. Biological applications of QDs as FRET donors have also been performed.[38–40] Steady-state and time-resolved fluorescence measurements have demonstrated that efficient nonradiative energy transfer between QD donors and organic dye acceptors has occurred, in a manner consistent with Forster theory.[39–45] Energy transfer has been observed between different QD–organic dye FRET pairs, when the QD acts as the donor fluorophore; target molecules have been nucleic acids, proteins, and other small molecules.[40,41,46,47] The spectral characteristics of QDs, such as their increased photostability, tunable emission spectra, and broad excitation spectra, make them extremely good candidates for donor fluorophores in a FRET reaction. However, the large size of QDs, including the QD core and the surface chemistry, may result in significant perturbation of the molecules under analysis. Therefore, the final organization and orientation of the molecules conjugated to QDs may be a significant problem when using quantum dots as FRET donors in biological applications. Significant heterogeneity in the orientation of the protein conjugates conjugated to the QD may yield a mixed functional behavior, resulting in a nonoptimal performance of the QD-protein conjugate as FRET donor.[38–41]

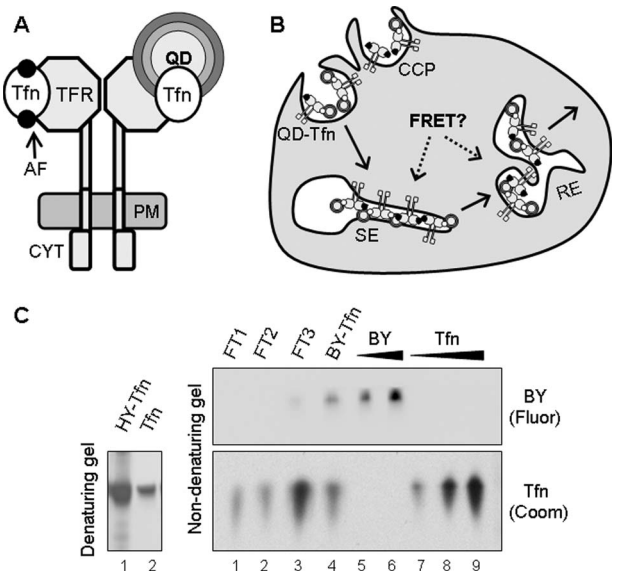

Fig. 1 Cell uptake of QD-Tfn donor and AF-Tfn acceptor molecules. (a) TFR dimer structure: Each apo-Tfn molecule binds two Fe^{3+} in the extracellular media. Two molecules of Tfn (iron-bound) bind each TFR dimer at the PM. In this particular example, one donor QD-Tfn and one acceptor AFTfn bind a TFR dimer. (b) Cellular system: TFR delivers QD-Tfn and AF-Tfn into cells. TFR-Tfn complexes are internalized via clathrin-coated pits (CCP) and delivered to sorting endosomes (SE) by clathrin-coated vesicles. Iron is released from Tfn as Fe^{2+} in the SE, and then the TFR-Tfn complexes are recycled back to the PM via recycling endosomes (RE). (c) Left panel: HY-Tfn conjugates and unlabeled Tfn were subjected to denaturing SDS-PAGE and Coomassie Blue analysis. Right panel: BY-Tfn conjugation was analyzed using nondenaturing PAGE, followed by Coomassie Blue and fluorescence imaging. Lanes 1 to 3: Flow-through (FT1-3) samples contain mainly unconjugated Tfn; lane 4: retentate solution contains predominantly BY-Tfn; lanes 5 to 6: increasing amounts of unconjugated BY; lanes 7 to 9: increasing amounts of unlabeled Tfn.

1.4 *FRET Analysis of TFR-Tfn Complexes in Endocytic Trafficking*

Transferrin-receptor (TFR) is involved in the iron uptake and delivery into the cells, a physiologically significant cellular process.[48,49] TFR behaves as a homodimeric type II transmembrane receptor; each TFR homodimer binds two molecules of iron-bound transferrin (Tfn) at the plasma membrane (PM) [Fig. 1(a); Refs. 48 and 50]. MDCK cells are a well-recognized biological model system to investigate the intracellular trafficking of membrane-bound receptors. TFR binds Tfn at the PM, and then TFR-Tfn receptor-ligand complexes are internalized into clathrin-coated vesicles and sorting endosomes, where endosome acidification induces the release of iron from Tfn. The majority of TFR-Tfn complexes are transported via recycling endosomes back to the PM [Fig. 1(b); Ref. 51].

Previously, the TFR-Tfn model system has been characterized using intensity-based FRET and the PFRET SBT correction algorithm.[24–26] The TFR-Tfn FRET-based assay showcases the capabilities of quantitative FRET analysis concerning the trafficking of membrane-associated receptor-ligand complexes.[24–26] As used here, TFR-Tfn complexes are a good FRET positive control for a typical clustered distribution due to their homo-dimeric nature, although we cannot

completely exclude the formation of higher-order clusters between TFR-Tfn receptor-ligand complexes.[24,26]

2 Material and Methods

2.1 *Growing MDCK Cells on Coverslips for Imaging*

Madin-Darby canine kidney (MDCK)–PTR cells, which express human TFR, are grown to confluence in 100-mm cell culture dishes.[25,52,53] After four days, the cells are trypsinized, centrifuged, and resuspended in Dulbecco's modified eagle medium (DMEM)/10% fetal bovine serum (FBS)/Pen-Strep. The cell suspension is then placed on coverslips, grown in DMEM/10% FBS/Pen-Strep for 18 to 24 h, and washed and used according to the appropriate internalization protocols (see the following).

2.2 *Conjugation of EviTag-QDs*

Tfn (iron-bound) was conjugated to primary amines on either Hops Yellow (HY; emission: 566 nm) or Birch Yellow (BY; emission: 580 nm) T2-MP EviTag QDs according to the manufacturer's instructions (http://www.evidenttech.com/life sciences/) resulting in HY-Tfn or BY-Tfn conjugates, respectively. Unbound Tfn was removed by centrifugation using a 100-K spin filter. HY-Tfn and BY-Tfn were characterized by Bradford protein quantitation assays (Biorad) and visualized by sodium dodecyl sulfate polyacrylamide gel electrophoresis (SDS-PAGE) and nondenaturing PAGE, followed by Coomassie Blue and fluorescence analysis using a Fuji-Film LAS-3000 viewer.

2.3 *Internalization of Fluorophore-Labeled Ligands*

Different amounts of BY-Tfn and AF594-Tfn (Invitrogen, Inc.) or HY-Tfn and AF568-Tfn (Invitrogen, Inc.) donor-acceptor pairs were incubated for 1 h at 37 °C with MDCK-PTR cells, previously equilibrated with DMEM/HEPES (4–(2–hydroxyethyl)-1–piperazineethanesulfonic acid)/BSA.[24,26,54] In both experiments, cells were washed with PBS to remove noninternalized QD-Tfn and AF-Tfn conjugates and then fixed with 4% paraformaldehyde/PBS. We have shown previously that cell fixation does not affect FRET behavior of TFR-Tfn receptor-ligand complexes.[24–26] For FRET measurements, three different samples were used: single-label reference donor samples containing either HY-Tfn or BY-Tfn, single-label reference acceptor samples containing AF568-Tfn or AF594-Tfn, and double-label specimens containing HY-Tfn and AF568-Tfn or BY-Tfn and AF594-Tfn conjugates, respectively. The donor and acceptor single-label reference samples are used to establish the SBT contamination levels when applying the correction PFRET algorithm (see the following).

2.4 *Laser Scanning Confocal FRET Microscopy*

Fixed cells were imaged using a Zeiss 510 META laser scanning confocal microscope, equipped with a 63× oil immersion lens 1.4 NA, and Argon (458-nm and 514-nm laser lines) and green HeNe (543 nm) lasers. LSM Zeiss software was used to drive the hardware, image acquisition, and processing.

Two different approaches were used to perform the FRET analysis of QD-Tfn as donors and AF-Tfn as acceptors. FRET images of single- and double-label cells containing HY-Tfn and/or AF568-Tfn were collected upon excitation with different laser lines, using different emission filters (BP535-590 or LP590) and the multitracking imaging function. The multitracking function was used to collect three images using: (1) 488-nm donor excitation and donor emission (BP535-590) channel—donor image; (2) 543-nm acceptor excitation and acceptor emission (LP590) channel—acceptor image; and (3) 488-nm donor excitation and acceptor emission (LP590) channel—FRET image. On the other hand, FRET images of single- and double-label cells containing BY-Tfn and AF594-Tfn were collected, upon excitation with 458-nm and 514-nm lasers, using lambda scans and spectral imaging to discriminate between donor and acceptor emission spectra. Lambda scans were performed using the LSM Zeiss META spectral detector to acquire lambda stacks, using 458-nm (donor) or 514-nm (acceptor) laser excitation lines; a 512×512 lambda stack is a stack of *x-y* images that sample emission data from a series of 10.7-nm wavelength bands from 505 nm to 719 nm. Lambda stack images, collected from cells containing BY-Tfn and/or AF594-Tfn, were processed by the LSM Zeiss linear unmixing proprietary algorithm to separate the donor from the acceptor emission spectra using reference spectra for BY-Tfn and AF594-Tfn. FRET spectral images correspond to acceptor emission images obtained by linear unmixing lambda stacks collected using the 458-nm donor laser excitation line. Imaging parameters, including laser power levels, pixel resolution (512×512), zoom (2×), pinhole size, detector gain and background levels, and imaging speed are kept constant for all channels and experiments throughout image collection.

2.5 *Post-Acquisition FRET Data Processing*

For background removal, measurements are performed on donor images collected from single-label acceptor samples and on acceptor images collected from single-label donor samples. For SBT correction using the PFRET algorithm, seven background-subtracted multitracking or spectral images are used: donor and FRET images from single-label donor samples; acceptor and FRET images from single-label acceptor samples; and three double-label images, acceptor, quenched donor (qD), and uncorrected FRET (uFRET).[23,24] ImageJ (http://rsb.info.nih.gov/ij/) software is used to open the laser scanning microscope (LSM) images collected using the Zeiss 510 META confocal microscope. Images are saved in 8-bit TIF format, and the average background is subtracted from each image.

After background removal, the PFRET algorithm removes the DSBT and/or ASBT contamination in a pixel-by-pixel manner on the basis of matched fluorescence levels between the double-label specimens and single-label reference specimens, as described previously.[23,27,29–31] The PFRET algorithm generates an image, named PFRET image, that represents the actual energy transfer (PFRET=uFRET−ASBT−DSBT). Then, PFRET software determines gray-level information in a pixel-by-pixel manner for acceptor, qD, uFRET, and energy transfer (PFRET) levels in preselected regions of interest (ROIs), having removed saturated donor pixels from the analysis. E% is calculated as a relative expression of the energy transfer as a percentage of the unquenched donor (D

$=qD+PFRET*\gamma$), as described in the following equation: $E\% = 100*(1-qD/D)$ Refs. 23, 24, 27, 30, and 55 The γ factor, which is a function of the quantum yield of the fluorophores and the spectral sensitivity of the detection setup, plays a crucial role in recording precise E% and distances between fluorophores. Since the excitation efficiencies (ε), quantum yields of the fluorophore molecules, and the detection efficiencies (Q) remain constant throughout each experiment, the γ factor does not affect the FRET quantitative analysis. Therefore, for simplicity, we have used $\gamma=1$, as described previously. [23–25,27,29] Nevertheless, it is important to notice that the relative E% values differ for data collected using distinct fluorophores or microscope systems.

3 Results and Discussion

3.1 *QD-Tfn Conjugates Track TFR-Mediated Internalization and Trafficking in Cells*

Fluorophore-labeled Tfn molecules have been widely used to follow the intracellular trafficking of TFR in MDCK-PTR cells.[24,25,54] Here, we have used EviTag QDs conjugated to Tfn molecules to track the intracellular endocytic trafficking of TFR-Tfn complexes as well as to evaluate the ability of QD-Tfn donor conjugates to transfer energy to AF-Tfn acceptor molecules during the endocytic pathway [Figs. 1(a) and 1(b)].[24,25] We have conjugated two different QDs to Tfn to generate QD-Tfn conjugates, HY-Tfn and BY-Tfn, as shown in Fig. 1(c).

EviTags are functionalized QDs that can be easily conjugated to proteins, antibodies, oligonucleotides and other biomolecules of interest using simple binding chemistries and easy-to-complete protocols. A standard protocol for conjugation was used as described by the manufacturer to generate purified EviTag QD-Tfn conjugates. In Fig. 1(c), we confirmed the presence of Tfn in the purified HY-Tfn conjugate by SDS-PAGE and Coomassie Blue staining. However, these denaturing conditions destroy the fluorescence properties of QDs. To verify the conjugation between QD and Tfn, we performed nondenaturing PAGE and assayed the Tfn levels by Coomassie Blue staining and the BY levels by fluorescence emission. As shown in Fig. 1(c), unbound Tfn is removed by centrifugation (FT1 to 3; lanes 1 to 3) using a 100-K spin filter, resulting in the accumulation of BY-Tfn in the concentrate solution (BY-Tfn; lane 4). In addition, image analyses of HY-Tfn and BY-Tfn drops were checked for aggregation (data not shown) and to collect their respective reference spectra. Only conjugates showing very low aggregation levels were used further in cell uptake assays.

To address whether HY-Tfn can be internalized into MDCK-PTR cells via TFR using a similar mechanism to that of Tfn, HY-Tfn was preincubated with excess amounts of unlabeled Tfn and then added to cells for 1 h at 37 °C. Upon internalization at 37 °C, HY-Tfn shows an intracellular as well as a cell surface distribution; in Fig. 2(a), arrows indicate punctate endocytic-like structures containing HY-Tfn located inside the cells. Competition with excess unlabeled Tfn leads to a markedly reduced internalization of HY-Tfn compared to that in the absence of unlabeled Tfn [Figs. 2(a) and 2(b)]. Moreover, in the presence of excess amounts of unlabeled Tfn, HY-Tfn labels mainly the cell surface [Fig. 2(b), arrows],

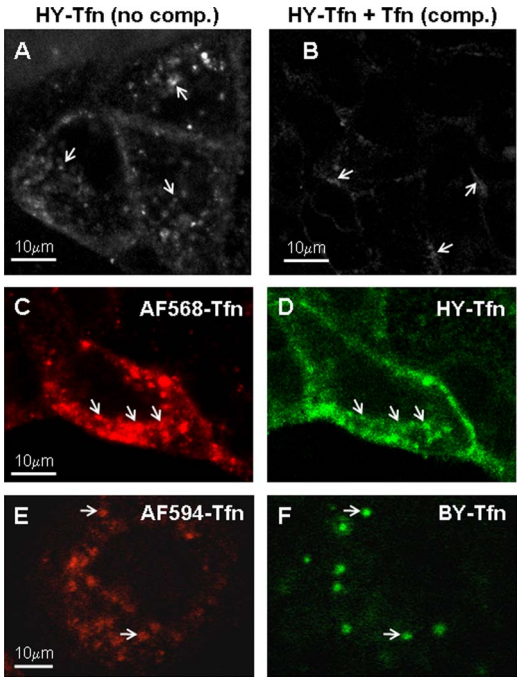

Fig. 2 Co-localization between QD-Tfn and AF-Tfn during endocytic pathway. (a) and (b) HY-Tfn was internalized into nonpolarized epithelial MDCK-PTR cells for 1 h at 37 °C in the presence (competition, comp.) or absence (no competition, no comp.) of excess unlabeled Tfn. Upon fixation, cells were mounted with glycerol and imaged using an LSM Zeiss 510 META confocal microscope using an emission filter-based approach. Importantly, in the absence of excess unlabeled Tfn, HY-Tfn was internalized into intracellular punctate endocytic-like structures (no comp., arrows). In contrast, in the presence of excess unlabeled Tfn, HY-Tfn internalization is significantly reduced; arrows indicate the nonspecific attachment of HY-Tfn to the cell surface (comp. panel). (c) and (d) HY-Tfn and AF568-Tfn were co-internalized into MDCK-PTR cells for 1 h at 37 °C, processed and imaged as described earlier. (e) and (f) BY-Tfn and AF594-Tfn were co-internalized into MDCK-PTR cells for 1 h at 37 °C and fixed and mounted with glycerol. Then, emission lambda scans were collected for BY-Tfn or AF594-Tfn with 458-nm or 514-nm laser excitation using an LSM Zeiss 510 META confocal microscope and processed by its linear unmixing software based on the reference emission spectra of AF594-Tfn and BY-Tfn to generate separate images that reflect the distribution of BY-Tfn (green) or AF594-Tfn (red) spectral signals. For (c) to (f) panels, overlapping staining (yellow) indicates the presence of QD and AF dyes in the same punctate structures (white arrows; merge panels); individual punctate structures may also contain just QD-Tfn (green; HY-Tfn or BY-Tfn panels) or just AF-Tfn (red; AF568-Tfn or AF594-Tfn). Bar: 10 μm. (Color online only.)

suggesting that it may be interacting nonspecifically with the cell surface. In summary, the competition assay indicates that the majority of HY-Tfn enters cells via TFR-mediated endocytosis in a way similar to that of unlabeled Tfn.

To test whether QD-Tfn and AF-Tfn conjugates follow similar endocytic trafficking pathways, HY-Tfn and AF568-Tfn were co-internalized into MDCK-PTR cells for 1 h at 37 °C and visualized by confocal microscopy using an emission filter-based imaging approach, as described previously for the receptor-mediated endocytosis of AF-Tfn conjugates.[24,26,54] The main difference between the HY-Tfn and AF568-Tfn distribution patterns is the stronger cell surface staining of HY-Tfn [Figs. 2(c) and 2(d). Several variables

such as the large size of the HY-Tfn conjugates, the number of Tfn per HY molecule, the iron-load level of HY-Tfn conjugates, and the nonspecific interaction of the HY surface layer with the PM may interfere with the efficiency of the HY-Tfn endocytosis leading to the observed increased amount of HY-Tfn that remains associated with the cell surface. Nevertheless, the strong co-localization of HY-Tfn and AF568-Tfn in intracellular punctate endocytic-like structures [Figs. 2(c) and 2(d), arrows], suggests that both HY-Tfn and AF568-Tfn are internalized and delivered to sorting endosomes, from where they can be recycled back to the PM via recycling endosomes.

A different QD-Tfn and AF-Tfn pair (BY-Tfn and AF594-Tfn) was incubated with MDCK-PTR cells for 1 h at 37 °C and visualized by confocal microscopy using a spectral imaging approach.[22,56,57] Spectral imaging and linear unmixing were used to separate the BY and AF594 emission spectra, which show overlapping emission peaks separated by more than 10 nm. A Zeiss 510 confocal microscope with a META spectral detector was used to acquire lambda stacks with 458-nm or 514-nm laser excitation lines from cells co-internalized with BY-Tfn and AF594-Tfn; reference spectra were collected from cells containing only BY-Tfn or AF594-Tfn. Then, the Zeiss linear unmixing algorithm was used to resolve the spectral signature in each pixel and assign different colors to the respective dyes in each pixel, resulting in the representation of the BY-Tfn and AF594-Tfn fluorescence signals in separate channels [Figs. 2(e) and 2(f)]. As expected, AF594-Tfn is internalized into endocytic-like structures, as shown previously [Fig. 2(e)].[24,26,54] Co-localization between BY-Tfn and AF594-Tfn in intracellular punctate endocytic-like structures [Figs. 2(e) and 2(f), arrows] suggests that both BY-Tfn and AF594-Tfn are internalized and delivered to the recycling endocytic pathway in a TFR-dependent manner [Figs. 2(e) and 2(f)]. Interestingly, BY-Tfn shows a reduced level of cell surface staining in comparison to that of HY-Tfn, suggesting some variability in the ability of different EviTag QD preparations to interact nonspecifically with the PM. However, BY-Tfn shows a lower level of uptake when compared to that of AF594-Tfn. As suggested for the internalization of HY-QD, different variables such as the large size of the QD-conjugates, the number of Tfn per BY EviTag QD, and the iron-load level of BY-Tfn conjugates may interfere with the efficiency of BY-Tfn endocytosis. Nevertheless, these results suggest that the majority of both BY-Tfn and HY-Tfn conjugates are able to track the internalization and trafficking of TFR molecules, using receptor-mediated endocytosis.

3.2 *QDs as FRET Donors*

CdSe-ZnS core-shell QDs have been used as donor molecules in *in vitro* and *in vivo* FRET assays.[37–39,58] To show as "proof of principle" that QDs can act as FRET donors upon uptake into cells, we have assayed the ability of QD-Tfn conjugates (donor) to transfer energy to AF-Tfn (acceptor) conjugates. As shown in Fig. 3(a), there is a significant spectral overlap between the emission of HY-Tfn and the excitation of AF568-Tfn, suggesting that HY and AF-568 make a good FRET pair. Similarly, the BY and AF594 also show a strong spectral overlap [Fig. 4(a)]. The R_0 values for the BY/AF594 and HY/AF568 FRET pairs (60 Å) were calculated in a similar

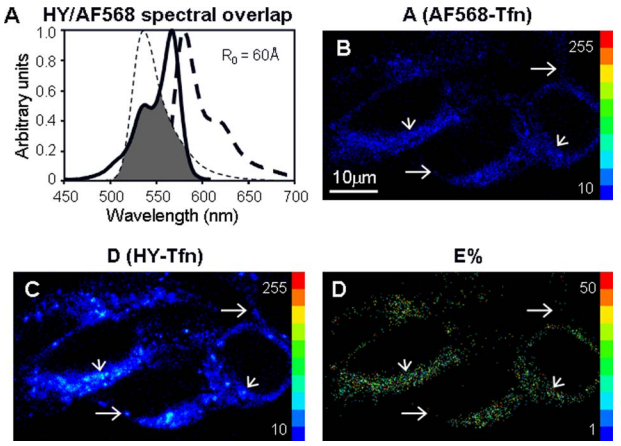

Fig. 3 Evidence of energy transfer between HY-Tfn and AF568-Tfn in cells. (a) HY versus AF568 emission spectra: HY emission (thin dotted line), AF568 excitation (thick line), and emission (thick dotted line) spectra. The significant spectral overlap (gray area) between donor emission (HY) and acceptor excitation (AF568) suggests a strong potential for FRET, which is confirmed by the R_0 value of 60 Å. (b) to (d) FRET imaging: Images from cells co-internalized with HY-Tfn and AF568-Tfn were collected using confocal microscopy and processed using the PFRET SBT correction algorithm to obtain pseudocolor images that depict the pixel-by-pixel distribution of A, D, and E% levels, showing significant energy transfer between HY-Tfn and AF568-Tfn in intracellular punctate structures. Areas with high D and A levels show strong E% levels (short arrows), whereas areas with high D but reduced A levels show low E% levels (long arrows).

manner using conventional FRET methodology,[37,40] and suggest that both HY and BY can act as strong donors for their respective AF acceptor partners.

To test whether FRET occurs between HY-Tfn and AF568-Tfn upon co-internalization into cells for 1 h at 37 °C, we collected filter-based FRET images as described earlier using 488-nm (donor) and 543-nm (acceptor) laser excitation lines. Then, the single-label and double-label images were processed for FRET intensity-based analysis using the PFRET algorithm[27] to remove the ASBT and DSBT from the uFRET image and generate the corrected PFRET image (data not shown) that contains the actual energy transfer levels.[23,27,29] In Figs. 3(b)–3(d), the pseudocolor image depicts acceptor (AF568-Tfn), unquenched donor (HY-Tfn), and E% in a pixel-by-pixel manner. The E% image shows significant energy transfer between BY-Tfn and AF594-Tfn in endocytic-like punctate structures containing both HY-Tfn and AF568-Tfn (short arrows), but not in structures containing only HY-Tfn (long arrows).

To test whether FRET occurs between BY-Tfn and AF594-Tfn upon binding to TFR and endocytosis into MDCK-PTR cells, we collected lambda stacks from single-label and double-label cells using 458-nm (donor) and 514-nm (acceptor) laser excitation lines and subjected them to linear unmixing as described earlier. Then, the single-label and double-label spectral images were processed for FRET intensity-based analysis using the PFRET algorithm[27] to remove the ASBT and DSBT from the uFRET image and generate the corrected PFRET image.[23,27,29] In Figs. 4(b)–4(d), the pseudocolor image depicts acceptor (AF594-Tfn), unquenched donor (BY-Tfn), and E% in a pixel-by-pixel manner. The E% image

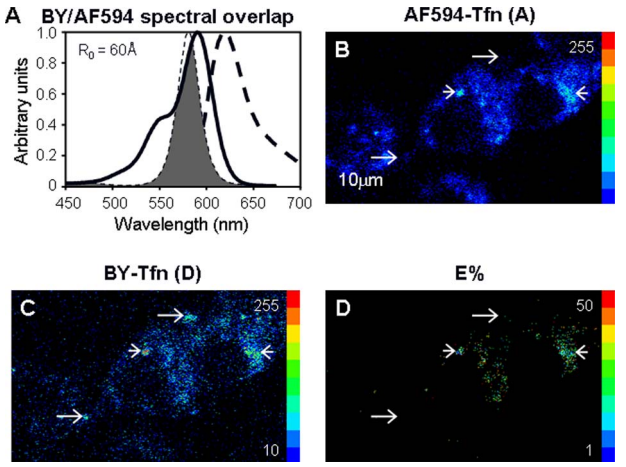

Fig. 4 Evidence of energy transfer between BY-Tfn and AF568-Tfn in cells. (a) Emission spectra of BY-Tfn and AF594-Tfn: BY-Tfn emission (thin dotted line) AF594-Tfn excitation (thick line), and emission (thick dotted line) spectra. The significant spectral overlap (gray area) between donor emission (BY-Tfn) and acceptor excitation (AF594-Tfn) suggests a strong potential for FRET, which is confirmed by the R_0 value of 60 Å. (b) to (d) FRET imaging: BY-Tfn or AF594-Tfn were co-internalized into MDCK cells for 1 h at 37 °C, fixed, mounted with glycerol, and imaged using an LSM Zeiss 510 META confocal microscope. Emission lambda scans for BY-Tfn or AF594-Tfn were collected and linear unmixed as described earlier. Then spectral images were processed using the PFRET SBT correction algorithm to obtain pseudocolor images that depict the pixel-by-pixel distribution of A, D, and E% levels, showing significant energy transfer between HY-Tfn and AF568-Tfn in intracellular punctate structures. Areas with high D and A levels show strong E% levels (short arrows), whereas areas with high D but low A levels show reduced E% levels (long arrows).

shows significant energy transfer between BY-Tfn and AF594-Tfn in endocytic-like punctate, structures containing both BY-Tfn and AF594-Tfn (short arrows), but not in structures containing only BY-Tfn (long arrows). In summary, the typical endocytic morphology of irregular, punctate, and peripherally localized structures and a centrally located nucleus is detected across all FRET images [Figs. 3(b), 3(d), 4(b), and 4(d)].

3.3 *Use of QDs Minimizes the Requirement for FRET SBT Correction*

Previously, we have demonstrated the necessity to implement SBT correction methods to generate correctly processed FRET results when using organic fluorophores as acceptor and donor molecules.[27] Here, by selecting a particular QD as a donor and an organic fluorophore as an acceptor together with filter-based or spectral imaging approaches, we can significantly reduce the SBT while preserving the strong spectral overlap necessary for FRET [Figs. 3(a) and 4(a)].

We subjected the HY-AF568 FRET pair to FRET confocal imaging and processing by the PFRET algorithm to measure the extent of SBT correction (i.e., the difference between uFRET and PFRET pixel intensity).[23,27,29] To discriminate the SBT due to the donor excitation of AF568-Tfn (ASBT) or to the HY-Tfn donor emission bleedthrough into the acceptor channel (DSBT), the PFRET algorithm was used to process uFRET images in the presence of only the acceptor or the donor single-label reference images, respectively [Figs. 5(a) and 5(b)]. As expected, a significant correlation (r-values >0.76) is detected between the PFRET and the uFRET values, independent of whether only ASBT, DSBT, or both are removed to generate the PFRET images [Fig. 5(a)].[24,26,27] These results suggest that there is a strong linear relationship between PFRET and uFRET values. In Fig. 5(b), a similarly strong correlation (r-values >0.79) is detected between the extent of SBT correction and the uFRET values, independent of whether only ASBT, DSBT, or both are removed. Another way to analyze the effect of ASBT and DSBT on the PFRET level is to determine the slope value for the PFRET or extent of correction versus uFRET relationships. Clearly, the slope values are higher ($s \sim 0.4–0.8$), suggesting a stronger relationship, when both ASBT and DSBT or only ASBT are removed than when only DSBT is removed ($s \sim 0.2$). These results suggest that the ASBT levels account for the majority of SBT correction using the PFRET algorithm ($\sim 70\%$). Moreover, this QD-AF FRET pair shows a high level of SBT correction ($\sim 80\%$), similar to that found for AF488-AF555 FRET pair (data not shown).

As shown in Fig. 4(a), the BY/AF594 shows a strong spectral overlap with reduced ASBT when using 458-nm laser for donor excitation to minimize the acceptor excitation. To reduce DSBT, we have used spectral imaging, which uses a linear unmixing algorithm to separate the donor and acceptor emission spectra, to remove the donor emission bleedthrough into the acceptor channel upon donor excitation. In Figs. 5(c) and 5(d), we have assessed the role of ASBT and DSBT in the PFRET and uFRET levels for the BY-AF594 FRET pairs when using spectral imaging and PFRET SBT correction approaches. A significant correlation (r-values >0.99) is detected between the PFRET and the uFRET values when ASBT, DSBT, or both are removed to generate the PFRET images [Fig. 5(c)], suggesting that there is a strong linear relationship between PFRET and uFRET values. A strong correlation (r-values >0.74) is detected between the extent of SBT correction and the uFRET values when DSBT or both ASBT and DSBT are removed [Fig. 5(d)]; in contrast, a lower correlation value is detected when only ASBT is removed (r-value ~ 0.48). Another way to analyze the effect of ASBT and DSBT on the PFRET level is to determine the slope value for the PFRET or extent of correction versus uFRET relationships. Importantly, the slope values are high ($s > 0.9$), independent of whether ASBT, DSBT, or both are removed. Furthermore, the slope values are significantly lower for the relationship between the extent of correction and uFRET ($s \sim 0.02$ to 0.1), indicating low levels of total SBT, including ASBT and DSBT. These results suggest that ASBT and DSBT levels account for ~55% versus ~45% of the total SBT correction using the PFRET algorithm, respectively. In contrast to HY-AF568 and AF488-AF555 high levels of SBT correction, the use of BY-AF594 as a FRET donor together with a spectral imaging approach leads to a major reduction in total SBT ($\sim 20\%$), keeping it at minimal levels.

In summary, using the HY-AF568 FRET pair together with emission filter-based image collection leads to reduced DSBT levels but still significant ASBT levels; thus, this FRET pair and imaging system would still require the use of a correction algorithm to process uFRET images. However, total SBT including ASBT and DSBT is reduced dramatically when the

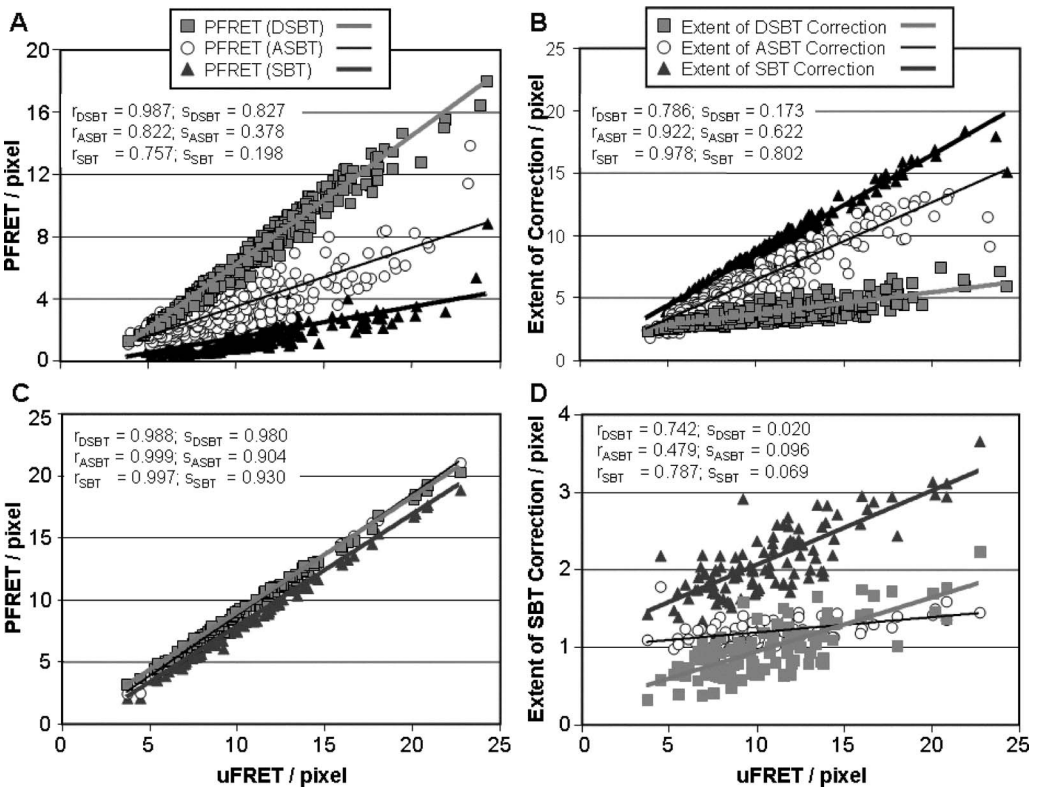

Fig. 5 Role of ASBT and DSBT in the extent of SBT correction after PFRET algorithm processing. These plots were obtained from ROI data collected from HY-AF568 FRET images [(a) and (b)] and BY-AF594 FRET images [(c) and (d)]; representative images are shown in Figs. 3 and 4, respectively. (a) and (c) PFRET versus uFRET levels after removal of ASBT (thin gray line and open circles), DSBT (thick gray line and gray squares), or both (black line and black triangle) using the PFRET algorithm; (b) and (d) the extent of SBT correction versus uFRET signal after removal of ASBT and/or DSBT using the PFRET algorithm. Trend lines are shown as visual aids. Correlation versus (*r*-values) and slope values (*s*-values) are shown.

BY-AF594 FRET pair is used together with 458-nm donor laser excitation (to reduce ASBT) and a spectral imaging approach (to minimize DSBT). These results suggest the importance of using spectral imaging approaches as well as carefully chosen QD-AF FRET pairs to take full advantage of the potential of QDs as donors for FRET experiments.

3.4 *Use of QDs as Donor Probes to Assay Receptor Clustering Using FRET*

To apply FRET quantitative analysis to the HY-Tfn/AF568-Tfn and BY-Tfn/Tfn-AF594 data sets, E% levels were plotted against acceptor levels, as described previously.[24–26] As shown in Figs. 6(a) and 6(b), E% behaves largely independently from acceptor levels for both FRET pairs. Correlation analysis substantiates this conclusion with a value of $r=0.1$ (HY-AF568) and $r=0.32$ (BY-AF594); as shown previously, r-values ≥ 0.5 show a significant positive dependency of E% on acceptor intensity levels, which indicates a random organization of the acceptor- and donor-labeled Tfn conjugates, whereas E%'s independence from acceptor levels leads to r-values < 0.5, suggesting a clustered distribution of TFR-Tfn receptor-ligand complexes.[24–26] Different E% levels for HY-AF568 versus BY-AF594 FRET pairs may be due to the D:A ranges used, D:A ~ 0.5 versus D:A ~ 2, as well as to the distinct imaging conditions. These results suggest that, as shown previously for Tfn-AF conjugates,[23–26] FRET between QD-Tfn and AF-Tfn conjugates is due to their clustered organization; energy transfer may occur between QD-Tfn and AF-Tfn conjugates bound to the same TFR homodimer (intramolecular FRET), or between QD-Tfn and AF-Tfn conjugates bound to different TFR molecules organized in higher-order clusters due to their co-internalization into similar endocytic trafficking pathways (intermolecular FRET).[24–26] These results showing a clustered distribution of QD-Tfn and AF-Tfn receptor-ligand complexes also excludes the possibility that a significant majority of QD-Tfn is entering the endocytic pathway via fluid-phase uptake, since soluble QD-Tfn should interact randomly with TFR-bound AF-Tfn. Considering the diameter of the EviTag QDs (15 to 25 nm), it is important to discuss their ability to transfer energy to AF acceptor molecules. An interesting hypothesis is that the coat, enveloping the EviTag core, displays a nonuniform diameter shell, which may explain the ability of these QDs to act as FRET donors to AF acceptors at distances that may be close to the R_0 values of these QD-AF FRET pairs.

3.5 *Summary*

Here, we have tested the ability of QDs to act as FRET donors and transfer energy to AF acceptors inside the cells using the TFR-Tfn FRET-based assay. QD FRET donors were coupled to Tfn and internalized into cells via TFR-mediated endocytosis. Then, a well-characterized quantitative FRET assay was used to detect the energy transfer between QD-Tfn donor conjugates and AF-Tfn acceptor conjugates during endocytic

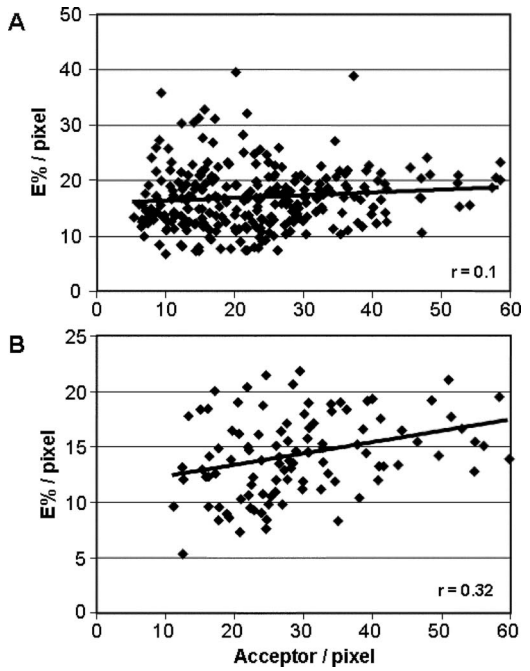

Fig. 6 Quantitative FRET analysis of QD-Tfn and AF-Tfn conjugates co-internalized into cells. (a) HY-Tfn and AF568-Tfn are co-internalized into MDCK-PTR cells for 1 h at 37 °C, imaged by filter-based confocal microscopy and processed for PFRET analysis. The A and E% values were extracted for a wide variety of ROIs and plotted against A levels at D:A~0.5 range. (b) BY-Tfn and AF594-Tfn are co-internalized into MDCK-PTR cells for 1 h at 37 °C, imaged by spectral confocal imaging and processed for FRET analysis using the PFRET algorithm. The A and E% values were extracted for a wide variety of ROIs and plotted against A levels at D:A~2 range. (a) and (b) E% is largely independent from A levels for both FRET pairs. Trend lines are shown as visual aids.

trafficking.[24–26] The FRET efficiency of two different QD-AF FRET donor-acceptor pairs was measured using emission filter-based as well as spectral-based confocal FRET imaging approaches and the PFRET SBT correction algorithm. Our results indicate that the FRET behavior of TFR-Tfn complexes occurs similarly in a manner independent of the QD-AF FRET pair used. However, QD conjugation to Tfn may hinder the specific binding of Tfn to TFR due to the large size of the QD and to the possibility that several Tfn molecules are bound to the same QD molecule. Using selective QD-AF FRET pairs allows for a significant reduction of the ASBT since QDs can be excited at wavelengths that minimize the acceptor excitation due to the broad excitation spectra of QDs. Spectral imaging, which uses a linear unmixing algorithm to separate the donor and acceptor emission spectra, can then be used as the sole methodology necessary to remove the donor emission bleedthrough into the acceptor channel upon donor excitation, i.e., DSBT.

3.6 *Technical and Biological Implications*

The significance of this research lies in the development of platform technology that will impact FRET-based imaging approaches designed to probe molecular mechanisms in live cells. Here, we have shown that the selective choice of QD-AF FRET pairs and imaging conditions may avoid the need to process FRET images to remove SBT. Such a development would allow the collection of real-time FRET images and data, which together with the increased photostability of QDs, would make real-time live-cell FRET a reality. In the future, new QD developments will draw upon the unique biophysical properties of QDs to eliminate much of the processing analysis required in determining E%; strengthen the quantitative data obtained in FRET imaging; make live-cell FRET imaging faster, brighter, and more quantitative; and allow for application of FRET-based approaches to tissue biology *in vivo* and *ex vivo*.

Acknowledgments

We would like to thank Evident Technologies, Inc., for their financial support, which allowed this work to be performed. We would also like to thank Alexandra Lacroix, Alyson Farrigton, Alfred Waring, and Daniel Landry for their strong support and insightful comments.

References

1. X. Gao and S. Nie, "Molecular profiling of single cells and tissue specimens with quantum dots," *Trends Biotechnol.* **21**, 371–373 (2003).
2. T. M. Jovin, "Quantum dots finally come of age," *Nat. Biotechnol.* **21**, 32–33 (2003).
3. W. C. Chan, D. J. Maxwell, X. Gao, R. E. Bailey, M. Han, and S. Nie, "Luminescent quantum dots for multiplexed biological detection and imaging," *Curr. Opin. Biotechnol.* **13**, 40–46 (2002).
4. W. W. Yu, E. Chang, R. Drezek, and V. L. Colvin, "Water-soluble quantum dots for biomedical applications," *Biochem. Biophys. Res. Commun.* **348**, 781–786 (2006).
5. H. Wallrabe and A. Periasamy, "Imaging protein molecules using FRET and FLIM microscopy," *Curr. Opin. Biotechnol.* **16**, 19–27 (2005).
6. P. Wu and L. Brand, "Resonance energy transfer, methods and applications," *Anal. Biochem.* **218**, 1–13 (1994).
7. L. Stryer, "Fluorescence energy transfer as a spectroscopic ruler," *Annu. Rev. Biochem.* **47**, 819–846 (1978).
8. L. Li, I. Gryczynski, and J. R. Lakowicz, "Resonance energy transfer study using a rhenium metal-ligand lipid conjugate as the donor in a model membrane," *Chem. Phys. Lipids* **101**, 243–253 (1999).
9. J. R. Lakowicz, *Principles of Fluorescence Spectroscopy*, 2nd ed., Kluwer Academic/Plenum Publishers, New York (1999).
10. T. Forster, "Delocalized excitation and excitation transfer," in *Modern Quantum Chemistry, Part III: Action of Light and Organic Crystals*, O. Sinanoglu, Ed., pp. 93–137 Academic Press, New York (1965).
11. V. S. Kraynov, C. Chamberlain, G. M. Bokoch, M. A. Schwartz, S. Slabaugh, and K. M. Hahn, "Localized Rac activation dynamics visualized in living cells," *Science* **290**, 333–337 (2000).
12. C. E. Chamberlain, V. S. Kraynov, and K. M. Hahn, "Imaging spatiotemporal dynamics of Rac activation *in vivo* with FLAIR," *Methods Enzymol.* **325**, 389–400 (2000).
13. G. W. Gordon, G. Berry, X. H. Liang, B. Levine, and B. Herman, "Quantitative fluorescence resonance energy transfer measurements using fluorescence microscopy," *Biophys. J.* **74**, 2702–2713 (1998).
14. P. I. Bastiaens and T. M. Jovin, "Microspectroscopic imaging tracks the intracellular processing of a signal transduction protein: fluorescent-labeled protein kinase, C beta I," *Proc. Natl. Acad. Sci. U.S.A.*, **93**, 8407–8412 (1996).
15. F. S. Wouters, P. I. Bastiaens, K. W. Wirtz, and T. M. Jovin, "FRET microscopy demonstrates molecular association of nonspecific lipid transfer protein (nsL-TP) with fatty acid oxidation enzymes in peroxisomes," *EMBO J.* **17**, 7179–7189 (1998).
16. L. Tron, J. Szollosi, S. Damjanovich, S. H. Helliwell, D. J. Arndt-Jovin, and T. M. Jovin, "Flow cytometric measurement of fluorescence resonance energy transfer on cell surfaces. Quantitative evaluation of the transfer efficiency on a cell-by-cell basis," *Biophys. J.*, **45**, 939–946 (1984).
17. C. Berney and G. Danuser, "FRET or no FRET: a quantitative comparison," *Biophys. J.* **84**, 3992–4010 (2003).
18. A. K. Kenworthy, "Imaging protein-protein interactions using fluo-

rescence resonance energy transfer microscopy," *Methods* **24**, 289–296 (2001).
19. M. M. Knight, S. R. Roberts, D. A. Lee, and D. L. Bader, "Live cell imaging using confocal microscopy induces intracellular calcium transients and cell death," *Am. J. Physiol.: Cell Physiol.* **284**, C1083–C1089 (2003).
20. S. Wu, D. Xing, F. Wang, T. Chen, and W. R. Chen, "Mechanistic study of apoptosis induced by high-fluence low-power laser irradiation using fluorescence imaging techniques," *J. Biomed. Opt.* **12**, 064015 (2007).
21. J. E. Vermeer, E. B. Van Munster, N. O. Vischer, and T. W. Gadella Jr., "Probing plasma membrane microdomains in cowpea protoplasts using lipidated GFP-fusion proteins and multimode FRET microscopy," *J. Microsc.* **214**, 190–200 (2004).
22. Y. Chen, J. P. Mauldin, R. N. Day, and A. Periasamy, "Characterization of spectral FRET imaging microscopy for monitoring the nuclear protein interactions," *J. Microsc.* **228**, 139–152 (2007).
23. H. Wallrabe, M. Elangovan, A. Burchard, A. Periasamy, and M. Barroso, "Confocal FRET microscopy to measure clustering of ligand-receptor complexes in endocytic membranes," *Biophys. J.* **85**, 559–571 (2003).
24. H. Wallrabe, Y. Chen, A. Periasamy, and M. Barroso, "Issues in confocal microscopy for quantitative FRET analysis," *Microsc. Res. Tech.* **69**, 196–206 (2006).
25. H. Wallrabe, G. Bonamy, A. Periasamy, and M. Barroso, "Receptor complexes cotransported via polarized endocytic pathways form clusters with distinct organizations," *Mol. Cell. Biol.* **18**, 2226–2243 (2007).
26. A. Periasamy, H. Wallrabe, Y. Chen, and M. Barroso, "Quantitation of protein-protein interactions: confocal FRET microscopy," *Methods Cell Biol.* (in press).
27. M. Elangovan, H. Wallrabe, Y. Chen, R. N. Day, M. Barroso, and A. Periasamy, "Characterization of one- and two-photon excitation fluorescence resonance energy transfer microscopy," *Methods* **29**, 58–73 (2003).
28. R. B. Sekar, and A. Periasamy, "Fluorescence resonance energy transfer (FRET) microscopy imaging of live cell protein localizations," *J. Cell Biol.* **160**, 629–633 (2003).
29. H. Wallrabe, M. Stanley, A. Periasamy, and M. Barroso, "One- and two-photon fluorescence resonance energy transfer microscopy to establish a clustered distribution of receptor-ligand complexes in endocytic membranes," *J. Biomed. Opt.* **8**, 339–346 (2003).
30. H. Wallrabe and M. Barroso, "Confocal FRET microscopy: Study of clustered distribution of receptor-ligand complexes in endocytic membranes," *Molecular Imaging, FRET Microscopy and Spectroscopy*, A. Periasamy and R. N. Day, Eds., pp. 95–111, Oxford University Press, New York (2005).
31. Y. Chen, M. Elangovan, and A. Periasamy, "FRET data analysis: the algorithm," in *Molecular Imaging, FRET Microscopy and Spectroscopy*, A. Periasamy and R. N. Day, Eds., pp. 126–145, Oxford University Press, New York (2005).
32. J. K. Jaiswal, H. Mattoussi, J. M. Mauro, and S. M. Simon, "Long-term multiple color imaging of live cells using quantum dot bioconjugates," *Nat. Biotechnol.* **21**, 47–51 (2003).
33. Y. T. Lim, S. Kim, A. Nakayama, N. E. Stott, M. G. Bawendi, and J. V. Frangioni, "Selection of quantum dot wavelengths for biomedical assays and imaging," *Mol. Imaging* **2**, 50–64 (2003).
34. A. M. Smith, X. Gao, and S. Nie, "Quantum-dot nanocrystals for *in vivo* molecular and cellular imaging," *Photochem. Photobiol.* **80**, 377–385 (2004).
35. D. S. Lidke, P. Nagy, R. Heintzmann, D. J. Arndt-Jovin, J. N. Post, H. E. Grecco, E. A. Jares-Erijman, and T. M. Jovin, "Quantum dot ligands provide new insights into erbB/HER receptor-mediated signal transduction," *Nat. Biotechnol.* **22**, 198–203 (2004).
36. K. Hanaki, A. Momo, T. Oku, A. Komoto, S. Maenosono, Y. Yamaguchi, and K. Yamamoto, "Semiconductor quantum dot/albumin complex is a long-life and highly photostable endosome marker," *Biochem. Biophys. Res. Commun.* **302**, 496–501 (2003).
37. A. R. Clapp, I. L. Medintz, and H. Mattoussi, "Forster resonance energy transfer investigations using quantum-dot fluorophores," *ChemPhysChem* **7**, 47–57 (2005).
38. I. L. Medintz, A. R. Clapp, H. Mattoussi, E. R. Goldman, B. Fisher, and J. M. Mauro, "Self-assembled nanoscale biosensors based on quantum dot FRET donors," *Nat. Methods* **2**, 630–638 (2003).
39. A. R. Clapp, I. L. Medintz, J. M. Mauro, B. R. Fisher, M. G. Bawendi, and H. Mattoussi, "Fluorescence resonance energy transfer between quantum dot donors and dye-labeled protein acceptors," *J. Am. Chem. Soc.* **126**, 301–310 (2004).
40. W. R. Algar, and U. J. Krull, "Quantum dots as donors in fluorescence resonance energy transfer for the bioanalysis of nucleic acids, proteins, and other biological molecules," *Anal. Bioanal. Chem.* (in press).
41. I. L. Medintz, J. H. Konnert, A. R. Clapp, I. Stanish, M. E. Twigg, H. Mattoussi, J. M. Mauro, and J. R. Deschamps, "A fluorescence resonance energy transfer-derived structure of a quantum dot-protein bioconjugate nanoassembly," *Proc. Natl. Acad. Sci. U.S.A.* **101**, 9612–9617 (2004).
42. I. L. Medintz, A. R. Clapp, H. Mattoussi, E. R. Goldman, B. Fisher, and J. M. Mauro, "Self-assembled nanoscale biosensors based on quantum dot FRET donors," *Nat. Mater.* **2**, 630–638 (2003).
43. I. L. Medintz, A. R. Clapp, F. M. Brunel, T. Tiefenbrunn, H. T. Uyeda, E. L. Chang, J. R. Deschamps, P. E. Dawson, and H. Mattoussi, "Proteolytic activity monitored by fluorescence resonance energy transfer through quantum-dot-peptide conjugates," *Nat. Mater.* **5**, 581–589 (2006).
44. I. L. Medintz, "Recent progress in developing FRET-based intracellular sensors for the detection of small molecule nutrients and ligands," *Trends Biotechnol.* **24**, 539–542 (2006).
45. A. R. Clapp, I. L. Medintz, and H. Mattoussi, "Forster resonance energy transfer investigations using quantum-dot fluorophores," *ChemPhysChem* **7**, 47–57 (2006).
46. I. L. Medintz, A. R. Clapp, F. M. Brunel, T. Tiefenbrunn, H. T. Uyeda, E. L. Chang, J. R. Deschamps, P. E. Dawson, and H. Mattoussi, "Proteolytic activity monitored by fluorescence resonance energy transfer through quantum-dot-peptide conjugates," *Nat. Mater.* **5**, 581–589 (2006).
47. A. R. Clapp, I. L. Medintz, and H. Mattoussi, "Forster resonance energy transfer investigations using quantum-dot fluorophores," *ChemPhysChem* **7**, 47–57 (2006).
48. Y. Cheng, O. Zak, P. Aisen, S. C. Harrison, and T. Walz, "Structure of the human transferrin receptor-transferrin complex," *Cell* **116**, 565–576 (2004).
49. C. M. Lawrence, S. Ray, M. Babyonyshev, R. Galluser, D. W. Borhani, and S. C. Harrison, "Crystal structure of the ectodomain of human transferrin receptor," *Science* **286**, 779–782 (1999).
50. D. R. Richardson, "Mysteries of the transferrin-transferrin receptor 1 interaction uncovered," *Cell* **116**, 483–485 (2004).
51. F. R. Maxfield, and T. E. McGraw, "Endocytic recycling," *Nat. Rev. Mol. Cell Biol.* **5**, 121–132 (2004).
52. E. Wang, P. S. Brown, B. Aroeti, S. J. Chapin, K. E. Mostov, and K. W. Dunn, "Apical and basolateral endocytic pathways of MDCK cells meet in acidic common endosomes distinct from a nearly neutral apical recycling endosome," *Traffic (Oxford, U. K.)* **1**, 480–493 (2000).
53. P. S. Brown, E. Wang, B. Aroeti, S. J. Chapin, K. E. Mostov, and K. W. Dunn, "Definition of distinct compartments in polarized Madin-Darby canine kidney (MDCK) cells for membrane-volume sorting, polarized sorting, and apical recycling," *Traffic (Oxford, U. K.)* **1**, 124–140 (2000).
54. M. Barroso, and E. S. Sztul, "Basolateral to apical transcytosis in polarized cells is indirect and involves BFA and trimeric, G protein sensitive passage through the apical endosome," *J. Cell Biol.* **124**, 83–100 (1994).
55. G. M. Bonamy, A. Guiochon-Mantel, and L. A. Allison, "Cancer promoted by the oncoprotein v-ErbA may be due to subcellular mislocalization of nuclear receptors," *Mol. Endocrinol.* **19**, 1213–1230 (2005).
56. Y. Chen, and A. Periasamy, "Localization of protein-protein interactions in live cells using confocal and spectral imaging FRET microscopy," *Indian J. Exp. Biol.* **45**, 48–57 (2007).
57. M. E. Dickinson, and G. Bearman, S. Tille, R. Lansford, and S. E. Fraser "Multi-spectral imaging and linear unmixing add a whole new dimension to laser scanning fluorescence microscopy," *BioTechniques* **31**, 1274–1276, (2001).
58. H. E. Grecco, K. A. Lidke, R. Heintzmann, D. S. Lidke, C. Spagnuolo, O. E. Martinez, E. A. Jares-Erijman, and T. M. Jovin, "Ensemble and single particle photophysical properties (two-photon excitation, anisotropy, FRET, lifetime, spectral conversion) of commercial quantum dots in solution and in live cells," *Microsc. Res. Tech.* **65**, 169–179 (2004).